Int. J. Electrochem. Sci., 10 **(2015)** 6572 - 6585

International Journal of
ELECTROCHEMICAL
SCIENCE
www.electrochemsci.org

Effect of Coarse Second-Phase Particles on Galvanic Corrosion of Anodized 6061 Aluminum Alloy Coupled with C1100 Copper

Liu-Ho Chiu[1], *Chi-Ying Tsai*[1], *Kuan-Hung Chen*[1], *Chia-Jung Hu*[1,*], *Heng Chang*[2]

[1] Department of Materials Engineering, Tatung University, 40 Chungshan N. Road, 3rd Sec., Taipei 10451, Taiwan
[2]Department of Mechanical Engineering, Chinese Culture University, Taipei 11114, Taiwan
[*]E-mail: cjhu@ttu.edu.tw

Received: 13 May 2015 / *Accepted:* 5 June 2015 / *Published:* 24 June 2015

This study investigated the effect of second-phase particles on the galvanic corrosion of anodized 6061 aluminum alloys coupled with C1100 copper alloys. The AA6061 alloys were solution treated at 530–570 °C for 1 h, followed by water quenching or furnace cooling. Anodic coatings of thicknesses 1, 5, and 12 μm were formed on AA6061-T6 after anodizing. The galvanic corrosion current of AA6061 coupled with C1100 copper was measured using a zero-resistance ammeter for 8 h in two solutions, namely 3.5 wt.% NaCl and 1.0 wt.% NaClO, at 25, 40, and 60 °C. Black Mg_2Si particles measuring 3−5 μm and white Al-Fe-Si-Cu particles measuring 3–8 μm were observed in the furnace-cooled AA6061 specimens. The highest galvanic corrosion current density (1312 μA/cm^2) in a flowing NaClO electrolyte was observed at 60 °C for the free-anodized AA6061-T6 alloy coupled with C1100 copper. The lowest galvanic corrosion current density (15 μA/cm^2) was observed in a 12-μm-thick anodic coating on AA6061-T6 alloy coupled with C1100 copper in a static 3.5 wt.% NaCl electrolyte at 25 °C. A severe corrosion attack was observed for a thin and nonuniform anodic coating on AA6061 alloy coupled with C1100 copper after the galvanic corrosion test because the coarse second-phase particles in the thin anodic coating on AA6061 caused perforations in the anodic coating. However, the thick anodic coating on AA6061 can effectively reduce the galvanic corrosion of AA6061-T6 coupled with C1100 copper in static or flowing electrolyte solutions.

Keywords: Aluminum alloy; Aging; Hard anodizing; Galvanic corrosion

1. INTRODUCTION

Aluminum and its alloys are widely used in numerous engineering applications and scientific technologies, such as aerospace, car engines, mechanical parts, and surface coating. The 6xxx series of aluminum alloys are commonly used in marine applications in which low density materials, high-

quality mechanical properties, and high resistance to corrosion are desired [1–3]. The resistance to corrosion of aluminum alloys is attributed to the formation of oxide (passive) films [4–6], which develop naturally on the alloy surface under normal atmospheric conditions. However, oxide films formed on the surface of aluminum alloys are thin, nonuniform, and noncoherent. Therefore, such films cannot provide adequate protection under corrosive conditions. Anodizing results in the creation of a thick oxidation coating on the alloy surface to protect it from corrosion [7–12].

AA6061 is a type of precipitation-hardening aluminum alloy. Second-phase particles in precipitation hardening aluminum alloys are typically classified into three types: constituents, dispersoids, and fine strengthening precipitates. The constituent phase particles are relatively large (2–5 μm) and primarily formed from the interaction of the alloying elements with impure elements such as Si and Fe. Dispersoids are relatively small (0.5–2 μm) and typically contain elements such as Mg, Cu, Zn, and Cr [13]. Differences in oxidation rates between the second-phase particles and aluminum substrate cause oxidation-free crevices at the particles/substrate interface in anodic coatings. Corrosive ions can attack the substrate through such crevices. Therefore, the second-phase particles in aluminum alloys play a major role in passivity breakdown and pit–morphology of aluminum alloys in seawater [14, 15]. In addition, Idrac [16] indicated that second-phase particles in an Al-Cu alloy resulted in pitting susceptibility in galvanic corrosion.

Direct contact between various metals commonly occurs in equipment that transmits liquids such as reclaimed water containing biocides including ClO^- and Cl^- ions. These types of water-system assemblies frequently combine aluminum alloys, copper alloys, stainless steel, low-alloy steel, and carbon steel [17]. Chloride ions can corrode these galvanic couples [18, 19]. In our previous paper [20], the preliminary investigation on the galvanic corrosion of anodized AA6061 alloys coupled with C1100 cooper. In this study, more and complete results evaluated the effect of precipitates in 6061 on the properties of anodized AA6061 in addition to the polarization corrosion and galvanic corrosion behavior of anodized AA6061 alloys coupled with C1100 Cu alloys in static or flowing ClO^- ion- or Cl^- ion-containing solutions.

2. EXPERIMENTAL PROCEDURES

2.1. Experimental materials

An AA6061 aluminum sheet was cut into several specimens measuring 2 × 25 × 80 mm. The composition of AA6061 was analyzed using an optical emission spectrometer (OES), as shown in Table 1. The specimens were solution treated at 530–570 °C for 1 h, followed by water quenching or furnace cooling. The water-quenched specimens were then aged at 180 °C for 8 h. The T6-aged specimens were anodized in 20 wt.% sulfuric acid solution with 6 g/L of $Al_2(SO_4)_3 \cdot 14–18H_2O$. The temperature of the electrolyte solution was maintained between −7 and −5 °C by using a chiller. The treatment was conducted at a constant current mode; the current density of the anode was 0.8 A/dm^2, and the fixed electrical parameters were unipolar rectangular pulses with a frequency of 1000 Hz, a

duty ratio of 0.6, and treatment times of 1, 5, and 12 min. The porous surface layers on the anodized specimens were sealed in 12 g/L of Ni $(CH_3COO)_2 \cdot 4H_2O$ at 80 °C for 5 min.

Table 1. Composition of sample compared with composition of AA6061 specification, wt.%

	Si	Fe	Cu	Mn	Mg	Cr	Zn	Ti	Al
Sample composition	0.73	0.48	0.21	0.07	0.81	0.17	0.09	0.07	Balance
AA6061 Specification	0.4~0.8	Max. 0.7	0.15~0.4	Max. 0.15	0.8~1.2	0.04~0.35	Max. 0.25	Max. 0.15	Balance

The surface and cross-sectional morphologies of the formed coating were measured using a scanning electron microscope (SEM) and an optical microscope (OM). The elemental concentration of the coatings was analyzed using an electron probe X-ray microanalyzer (EPMA).

2.2. Potentiodynamic polarization test

The corrosion behaviors of the samples were evaluated using potentiodynamic polarization (Solartron SI 1287 Electronchemical interface) in 3.5 wt.% NaCl solution (pH = 7) or 1.0 wt.% NaClO solution (pH = 10) with a silver/silver chloride electrode (SSE) and platinum serving as reference and counter electrodes, respectively. The samples were mechanically polished using 800-grit waterproof abrasive paper and then ultrasonically degreased in acetone and distilled water. The sample potential was swept at a rate of 1 mV/s from the initial potential of −0.3 V to the final potential of +0.8 V versus an open-circuit potential (OCP). Before testing, the specimen was soaked in an electrolyte solution for some time until the OCP value stabilized. The corrosion potential and corrosion density were analyzed using Tafel extrapolation.

2.3. Galvanic corrosion test

According to the ASTM G71–81 specification [21], the galvanic current of an anodized 6061 aluminum plate coupled with C1100 copper alloy was measured using a zero-resistance ammeter. The specimens were mechanically polished using 800-grit waterproof abrasive paper, ultrasonically degreased in acetone, and dried. The galvanic corrosion tests for the couple were conducted using the two electrolytes from the polarization test at 25, 40, and 60 °C. The galvanic corrosion test was conducted continuously during an 8-h period.

3. RESULTS AND DISCUSSION

3.1. Microstructure analysis

Second-phase particles were observed in the 6061 specimens after a solution treatment at 530 °C for 1 h, followed by furnace cooling or water quenching. Figure 1 shows the microstructures of

furnace-cooled and water-quenched specimens. As shown in Figure 1a, many black particles of size approximately 3−5 μm and white particles of size approximately 3−8 μm were observed in the furnace-cooled specimen. Black particles were almost absent in the water-quenched specimen, whereas the white particles were present in it (Figure 1b).

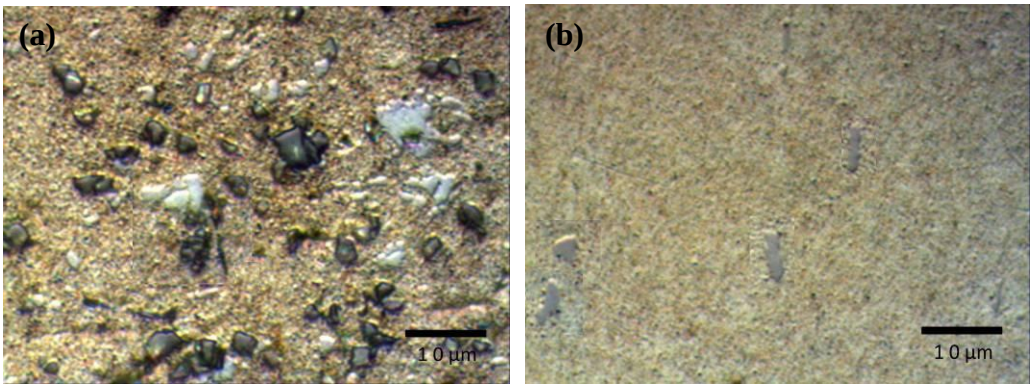

Figure 1. Microstructures of AA6061 treated using (a) furnace cooling and (b) water quenching.

The black particles in the water-quenched specimen were considerably less and smaller than those in the furnace-cooled specimen. The results of the EPMA analysis indicated the existence of two particle phases in the specimens.

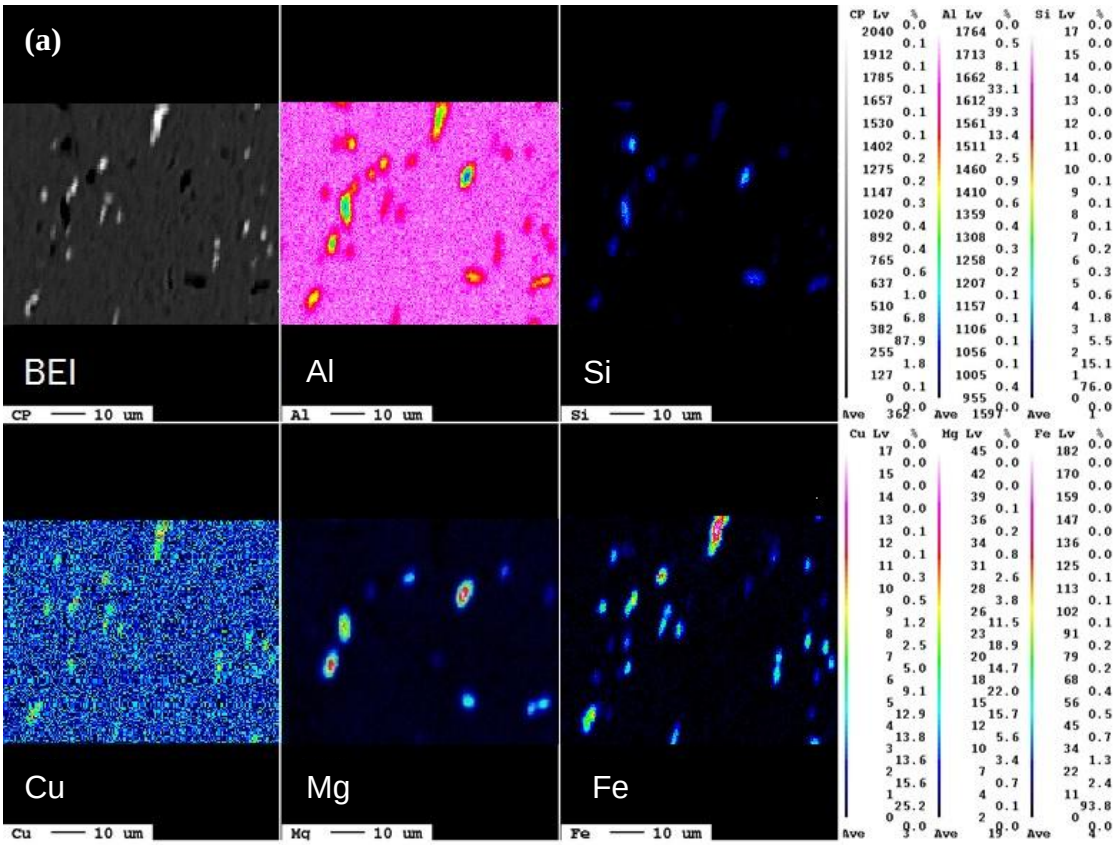

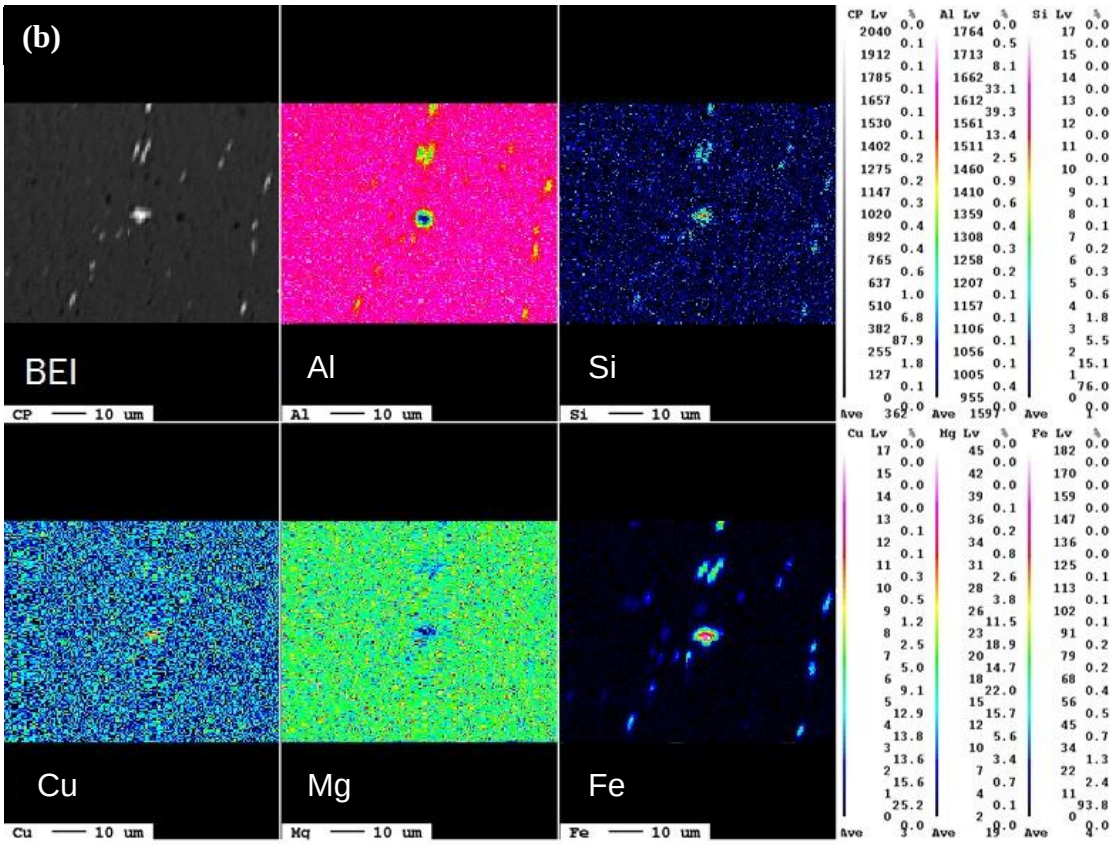

Figure 2. BEI and element maps of (a) furnace-cooled and (b) water-quenched AA6061.

Figure 2 shows a backscattered electron image (BEI) and element maps of furnace-cooled and water-quenched AA6061 specimens. A black particle measuring approximately 3–5 μm and white particle measuring approximately 3–8 μm coexisted in the furnace-cooled specimen (Figure 2a). According to the element mappings, the black particles primarily comprised Mg and Si elements, implying that black particles, namely Mg_2Si, precipitated during the furnace cooling process. Conversely, Fe, Cu, Al, and Si were the dominant elements in the white particles, indicating that the white particles were Al-Fe-Si-Cu-containing precipitates. The quantity and size of black particles clearly decreased in the water-quenched specimen, whereas the constituent white particles were easily observed (Figure 2b). A previous study [22] indicated that in 6xxx series alloys, the major intermetallic phase particles are primarily Fe-rich intermetallic particles and Mg_2Si precipitates.

Figure 3 depicts anodic coatings of thicknesses 3–5 μm (Figure 3a) and 15–18 μm (Figure 3b) on AA6061-T6, which included precipitate particles. Perforation-like areas were observed in the hard anodic coating with a thickness of 3–5 μm. The areas comprised extremely few O and Al elements, which were confirmed using energy-dispersive X-ray spectroscopy (EDS), indicating that the areas were perforations in the coating. Moreover, Fe, Si, and Cu elements were observed near the perforation, implying that the perforation nucleated at the AlFeSiCu particle/Al-substrate interface during anodizing. Because the Fe-rich intermetallic particles have a high electrochemical potential compared with the aluminum matrix [23, 24], which are more difficult to be oxidized than an Al-substrate during anodizing, it resulted in the perforation of the hard anodic coating near the precipitates. The EDS

analysis results confirmed that the white precipitate particles in the coatings represented an Al-Fe-Si compound comprising 92.2% Al, 4.5% Fe, and 2.5% Si (Figure 3a). In addition, the hard anodic coating was perforated when Fe-rich intermetallic particles precipitated in the substrate, resulting in a rougher surface.

White Al-Fe-Si particles measuring approximately 3 μm were embedded in a hard anodic coating of thickness 15–18 μm (Figure 3b). In addition, black particles measuring approximately 3 μm consisted of 72.7% Al, 20.2% Si, and 7% Mg, confirmed by the EDS analysis, implying that they may be Mg_2Si precipitates. The EDS analysis shows that the primary composition of the aluminum substrate is 99.2% Al and small amounts of Mg and Si (Figure 3b). The size of the precipitate particles remained unchanged (Figure 3) compared with those of the specimens before aging or anodizing (Figures 1 and 2). White precipitate particles existed in the inner 50% of the anodic coating thickness and substrate; however, the particles were almost absent in the outer 50% of the anodic coating thickness (Figure 3b), suggesting that the anodic coating is a product of the chemical conversion of the substrate metal into its oxide and grows both inward and outward from the original metal surface [25, 26]. During the anodizing process in electrolytes, the anodic coating grows at the alloy/coating interface through inward migration of O^{2-}/OH^{-} ions; outwardly mobile Al^{3+} ions are ejected at the pore/base coating interface [27–29]. Therefore, no perforation exists in the hard anodic coating because it is sufficiently thick (i.e., 15–18 μm), as shown in Figure 3b.

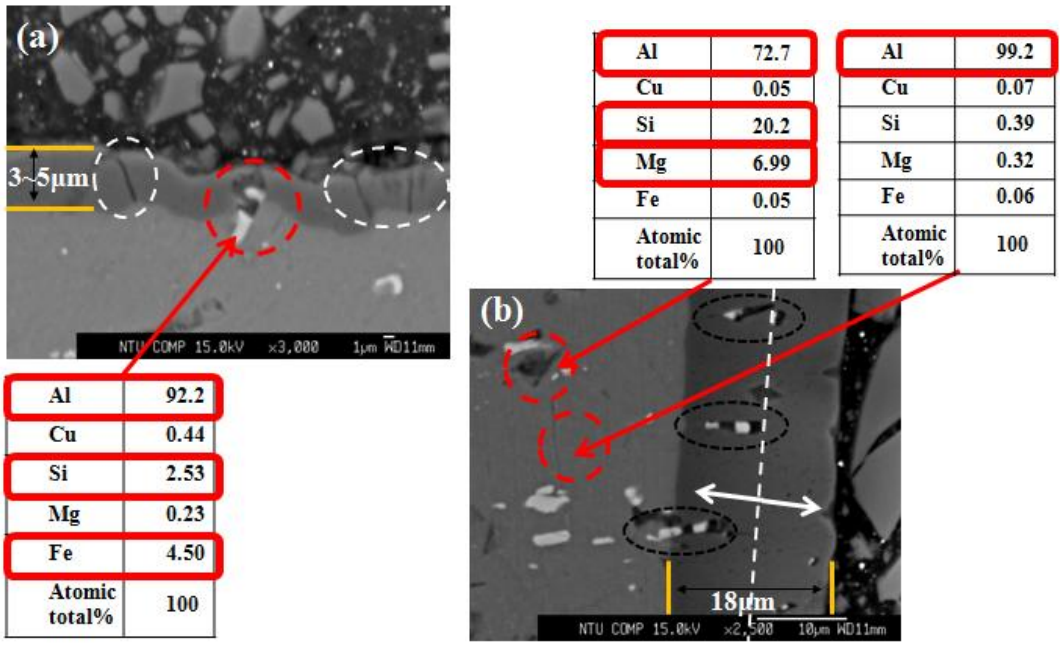

Figure 3. SEM and EDS analysis of anodic coatings of thicknesses (a) 3–5 μm and (b) 18 μm on AA6061.

3.2. Polarization test

Figure. 4 depicts the polarization curves of the AA6061 samples at given conditions in 3.5 wt.% NaCl (pH = 7) and 1.0 wt.% NaClO (pH = 10) aqueous solutions. Figures 5 and 6 show a

summary of the corrosion potentials and corrosion current densities of the polarization tests. The corrosion potentials of AA6061-T6 in the NaCl and NaClO solutions were −0.68 and −1.19 V, respectively, suggesting that this alloy was more active in corroding AA6061 alloy in the NaClO solution than it was in the NaCl solution. The corrosion current densities of AA6061-T6 in the NaCl and NaClO solutions were 1.09×10^{-6} and 5.13×10^{-6} A/cm², respectively. These values are higher than that of pure Al (i.e., 7.12×10^{-7} A/cm²) because the corrosion rate of AA6061 increased with the concentration of alloying elements in the alloy [16]. The corrosion current densities of the anodized specimens with the oxide film of thickness 1 μm were 1.69×10^{-6} and 8.66×10^{-7} A/cm^2 in the NaCl and NaClO solutions, respectively. In other words, the approximately 1-μm-thick anodic coating on AA6061 was not sufficient to improve its corrosion resistance because of some perforations in the coatings. For the anodized specimens with oxide coating having a thickness of approximately 5 μm, the corrosion current densities in the NaCl and NaClO solutions were 5.67×10^{-7} and 1.48×10^{-8} A/cm^2, respectively.

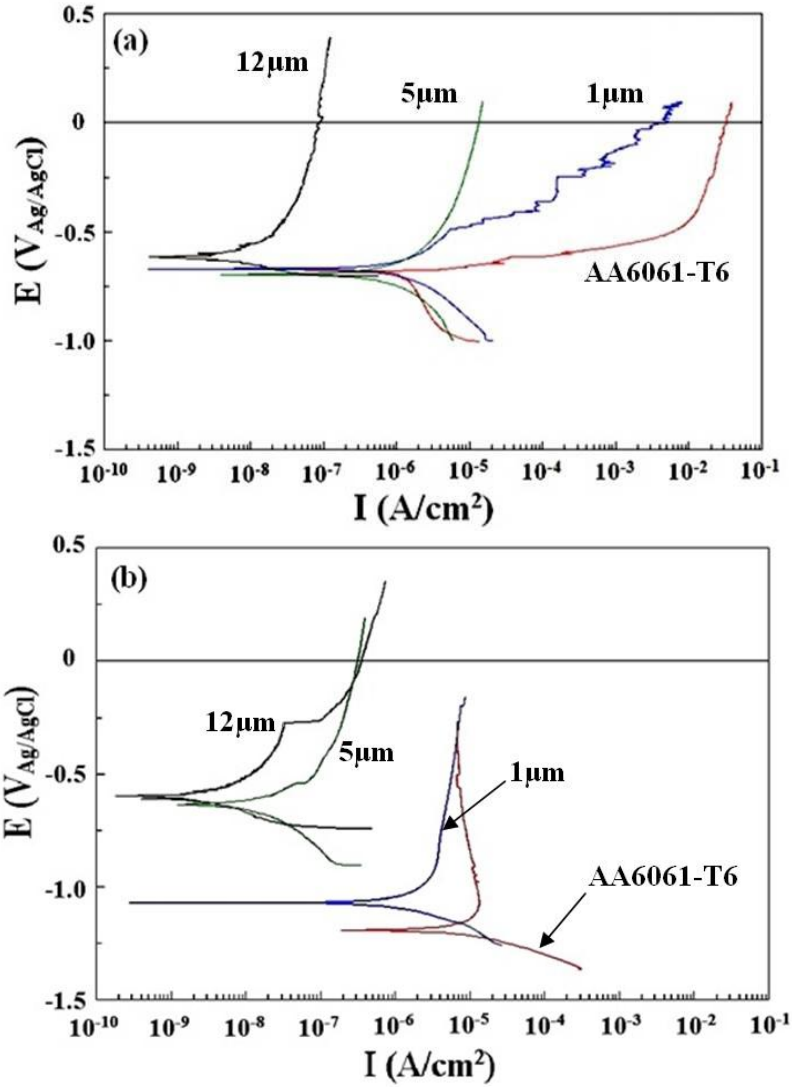

Figure 4. Polarization curves of as-T6-treated AA6061, followed by anodizing specimens in (a) 3.5 wt.% NaCl and (b) 1.0 wt.% NaClO aqueous solutions, respectively.

The corrosion resistance of the AA6061 plate can be improved using a thicker oxide coating. When the anodic coating thickness was increased to 12 μm, the corrosion current densities in the NaCl and NaClO solutions were 2.17×10^{-9} and 1.90×10^{-9} A/cm^2, respectively. The corrosion current density considerably decreased when the anodic coating thickness increased. An anodic oxide film with a thickness of approximately 12 μm can adequately protect AA6061 from corrosion. The corrosion resistance of AA6061-T6 was improved because it was coated with a uniform and dense anodic coating of thickness greater than 12 μm.

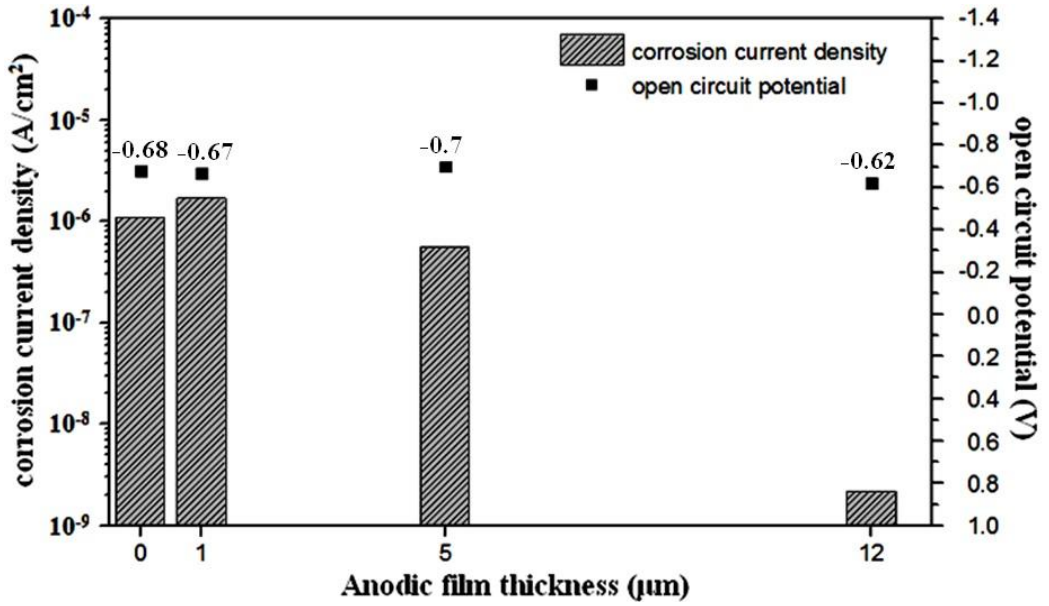

Figure 5. Corrosion potential and corrosion current density of anodized AA6061-T6 in a 3.5 wt.% NaCl solution.

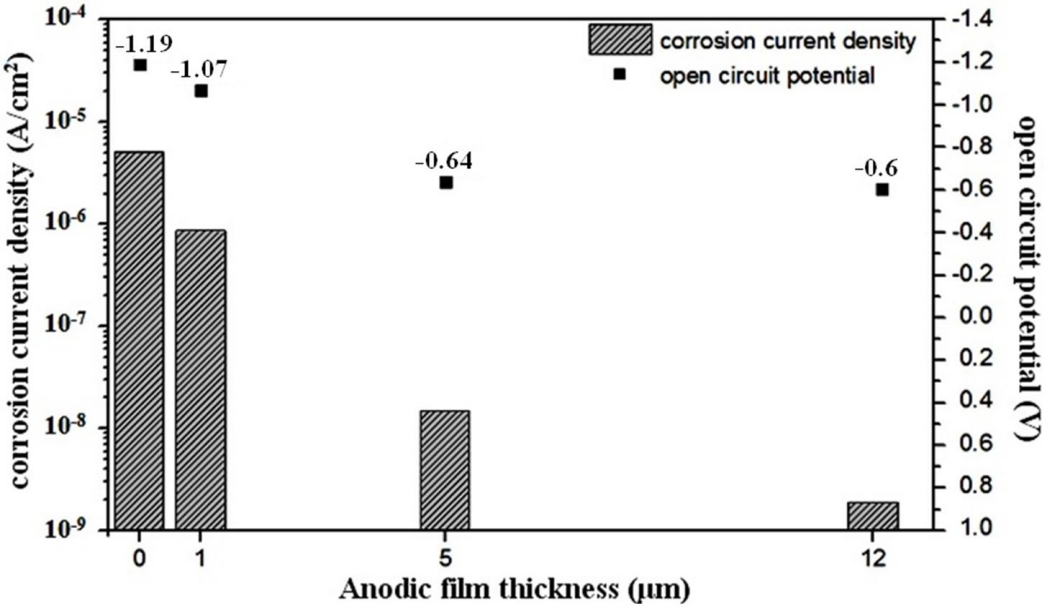

Figure 6. Corrosion potential and corrosion current density of anodized AA6061-T6 in a 1.0 wt.% NaClO solution.

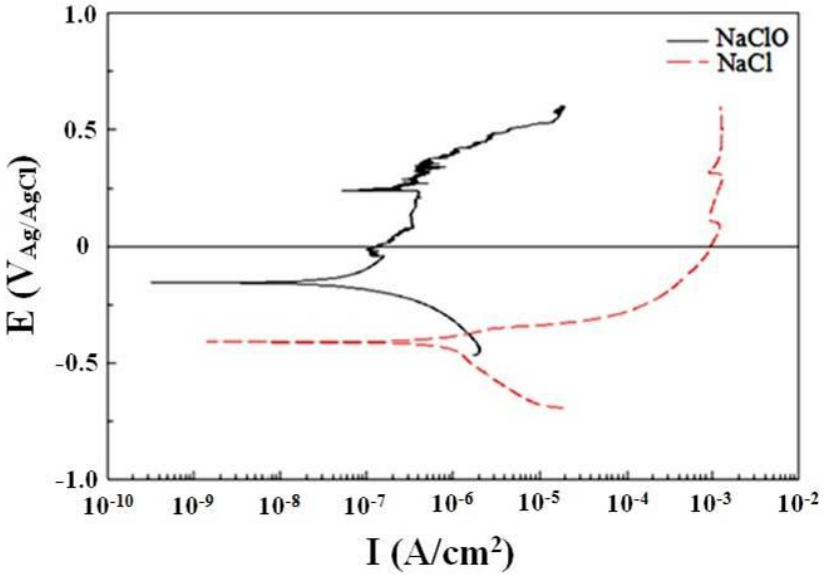

Figure 7. Polarization curves of the C1100 Cu plate specimen in 3.5 wt.% NaCl and 1.0 wt.% NaClO aqueous solutions, respectively.

Table 2 indicates that the corrosion potentials and corrosion current densities of the C1100 Cu plate in the NaCl and NaClO solutions are −0.41 and −0.15 V and 6.33×10^{-7} and 8.17×10^{-8} A/cm², respectively. Polarization corrosion can be used to predict the galvanic corrosion of an AA6061 plate coupled with C1100 copper. According to the corrosion potentials of AA6061-T6 and C1100 copper, the difference in the corrosion potential between the aluminum alloy and copper in the 3.5 wt.% NaCl solution is lower than that in the 1.0 wt.% NaClO solution (Figures 4−7 and Table 2), suggesting that the galvanic corrosion current density of 6061 coupled with C1100 copper in the 3.5 wt.% NaCl solution should be lower than that in the 1.0 wt.% NaClO solution. Zaid [30] indicated that the corrosion rate of AA6061 in neutral solutions (pH = 6) is lower than that in alkaline chloride (pH = 12) or in acidic (pH = 2) solutions. The corrosion of the Al matrix in neutral and alkaline media is closely dependent on the formation of aluminum hydroxide (Al $(OH)_3$) as a protective layer [30]. The oxide film is dissolved by a chemical reaction, which is catalyzed by the presence of a high OH^- concentration in alkaline solutions [31–33]. Therefore, the higher galvanic corrosion current density of AA6061 coupled with C1100 copper was possibly attributed to a higher OH^- concentration in the 1.0 wt.% NaClO solution than in the 3.5 wt.% NaCl solution, suggesting that the galvanic corrosion of AA6061 coupled with C1100 copper is more active in biocide water than in seawater.

Table 2. Corrosion potentials and corrosion current densities of the C1100 Cu plate specimens in 3.5 wt.% NaCl and 1.0 wt.% NaClO aqueous solutions, respectively.

solution	corrosion potential (V)	corrosion current density (A/cm^2)
3.5 wt. % NaCl	-0.41	6.33×10^{-7}
1.0 wt. % NaClO	-0.15	8.17×10^{-8}

3.3. Galvanic corrosion test.

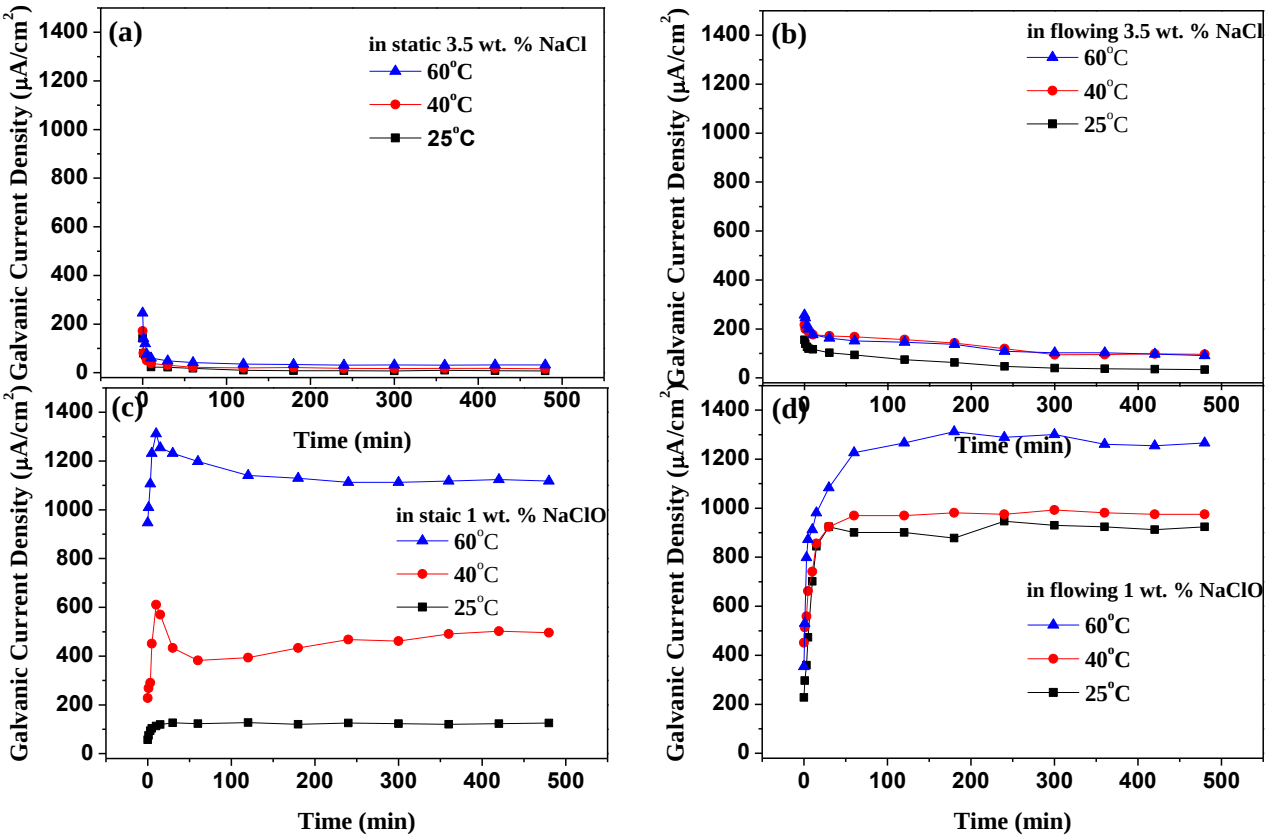

Figure 8. Variation of galvanic current densities with time for AA6061 coupled with C1100 Cu at various temperatures in (a) static and (b) flowing 3.5 wt.% NaCl aqueous solutions and in (c) static and (d) flowing 1.0 wt.% NaClO aqueous solutions.

Figure 8 shows the galvanic current densities of AA6061-T6 coupled with C1100 copper in 3.5 wt.% NaCl and 1.0 wt.% NaClO static and flowing aqueous solutions, respectively. The galvanic corrosion current density of AA6061 coupled with C1100 cooper in the 1.0 wt.% NaClO solution was higher than that in the 3.5 wt.% NaCl solution, which was confirmed by a higher corrosion potential difference between the aluminum alloy and copper in the 1.0 wt.% NaClO solution than that in the 3.5 wt.% NaCl solution (Table 2). In a 3.5 wt.% NaCl solution, the corrosion rate decreases with increasing exposure time, irrespective of a static or flowing solution. The galvanic current density of the AA6061 plate coupled with a C1100 plate in a flowing state is greater than that in a static state in both aqueous solutions. In a static solution, the corrosion rate is a function of exposure time. For an extended period, the corrosion can stop when the corrosion product reaches its equilibrium concentration. This is not true for a flowing solution. The flowing liquid can transport the corrosion products away from the metal surface and bring the reactants to the metal surface, thus accelerating the dissolution process [34]. As indicated by Balbaud-Celerier [35], the corrosion rates increase with the flow velocity in mass transfer controlled regimes. Figure 8d shows that the galvanic corrosion current

density of AA6061-T6 coupled with C1100 copper under a flowing NaClO electrolyte at 60 °C exhibits the highest value (1312 μA/cm^2) among the various temperatures.

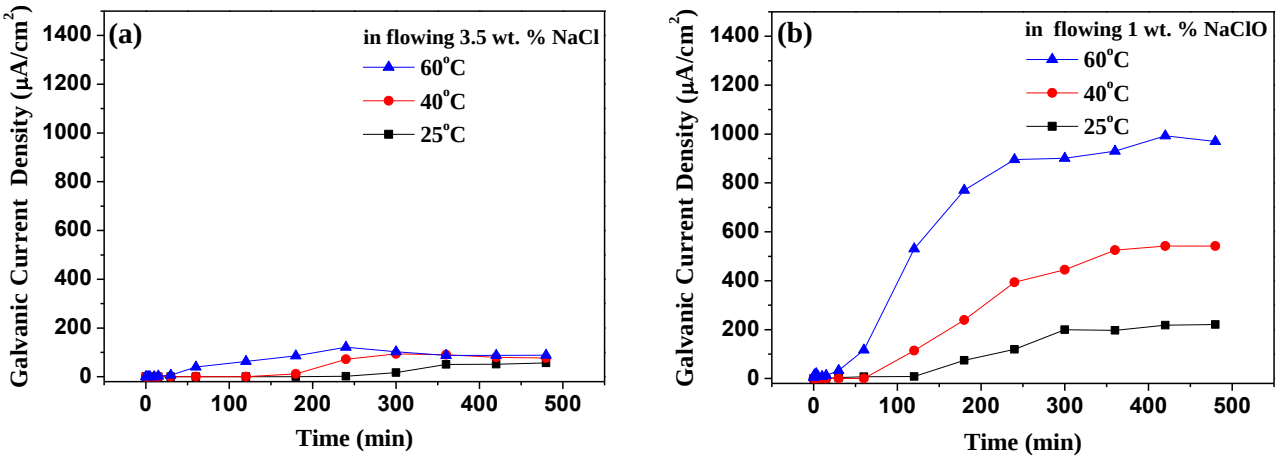

Figure 9. Variation of galvanic current density with time for a 12-μm-thick hard coating on an AA6061 plate coupled with C1100 Cu alloy at different temperatures in (a) 3.5 wt.% NaCl and (b) 1.0 wt.% NaClO flowing aqueous solutions.

Figure 9 indicates that the galvanic corrosion current density of an anodized AA6061 plate coupled with C1100 copper in a flowing NaClO electrolyte at 60 °C has the highest value (970 μA/cm^2) among the various temperatures, which is considerably lower than that of the as-T6-treated AA6061 coupled with C1100 copper (312 μA/cm^2). No galvanic current densities of the anodized alloy coupled with copper were observed for up to 30 or 60 min, indicating that the anodic coatings adequately protected the aluminum substrate against corrosive agents.

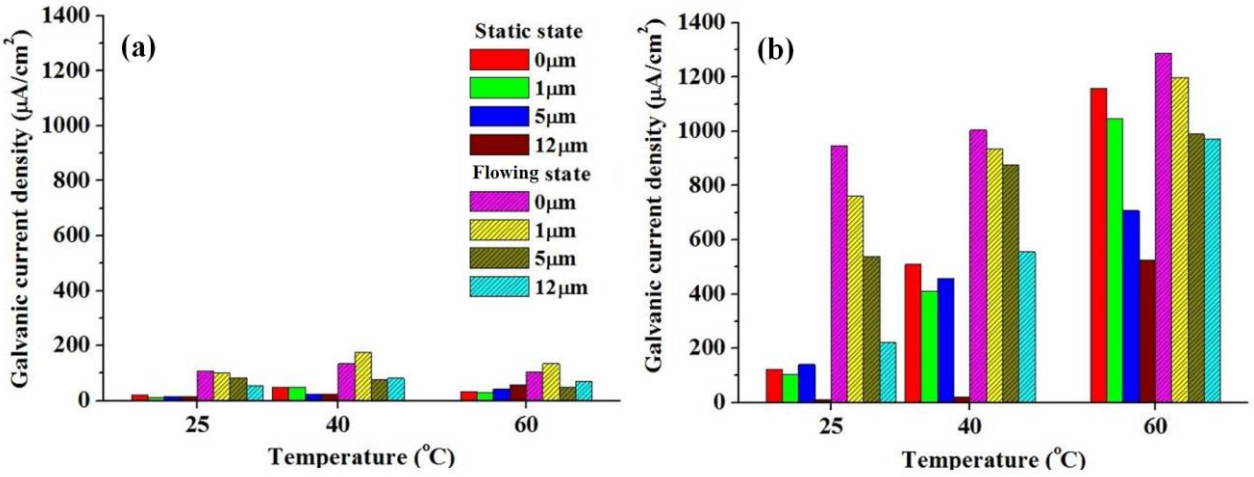

Figure 10. Effect of electrolyte temperature and anodic coating thickness on galvanic corrosion current density of anodized AA6061 coupled with C1100 Cu in (a) 3.5 wt.% NaCl and (b) 1.0 wt.% NaClO static and flowing aqueous solutions.

Moreover, the highest galvanic corrosion current density (100 μA/cm^2) of the anodized alloy coupled with copper in the flowing NaCl solution was considerably lower than that of the as-T6-treated AA6061 coupled with C1100 copper (300 μA/cm^2).

Fig. 10 illustrates the effect of electrolyte temperature and anodic coating thickness on the galvanic corrosion current density of anodized AA6061 coupled with C1100 Cu. The 12-μm-thick anodic coating on AA6061-T6 coupled with C1100 copper demonstrated the lowest galvanic corrosion current (15 μA/cm^2) in the static 3.5 wt.% NaCl electrolyte at 25 °C. A severe corrosion attack occurred in the 1- and 5-μm-thick anodic coatings on the AA6061-T6 specimens after the galvanic corrosion tests because of some perforations in the anodic coatings. The galvanic corrosion current density increased with the temperature of the electrolyte solution. The galvanic current densities decreased as the anodic coating thickness increased. In other words, the sufficiently thick anodic coating acts as a protector for this alloy against corrosive agents.

4. CONCLUSIONS

This study investigated the effects of second-phase particles, electrolyte temperature, and anodic coating thickness on the galvanic corrosion behaviors of anodized AA6061 coupled with C1100 copper in static and flowing NaCl and NaClO solutions.

1. Numerous black Mg_2Si particles measuring 3–5 μm, and white Al-Fe-Si-Cu constituent phase particles measuring 3–8 μm were observed in the furnace-cooled AA6061 specimens. The black particles were not retained in the water-quenched specimen, whereas the white particles were retained. The corrosion current density of AA6061-T6 in a 3.5 wt.% NaCl solution was less than that in a 1.0 wt.% NaClO solution.
2. The corrosion current density decreased considerably because of the existence of a thick anodic layer on this alloy, indicating that a dense and uniform 12-μm-thick anodic coating can adequately protect the aluminum substrate against corrosive agents.
3. The type of corrosive solution, state (static or flowing), and electrolyte temperature are the factors of the galvanic corrosion current density of this alloy. During prolonged erosion, a flowing state and higher electrolyte temperature caused more galvanic corrosion on the anodized aluminum alloy coupled with copper.
4. A severe corrosion attack was observed in the 1- and 5-μm-thick anodic coatings on the AA6061-T6 specimens after the galvanic corrosion tests; this attack was caused by the existence of perforations in the anodic coatings. However, the thick anodic coating on AA6061 can effectively reduce the galvanic corrosion of AA6061-T6 coupled with C1100 copper in static or flowing electrolyte solutions.

ACKNOWLEDGMENTS

The authors thank the National Science Council, Republic of China, for financially supporting this study under grant NSC 101-2622-E-036-005-CC3. Partial financial support was provided by the

Gateway Asian Sourcing Corp. In addition, the authors thank C.Y. Kao of the Instrumentation Center of National Taiwan University for his EPMA support.

References

1. J. Davis, editor, *Corrosion of Aluminum and Aluminum Alloys,* USA: ASM International, (1999) 25
2. E. Hollingsworth and H. Hunsicker, *Metals Handbook*, 9th ed., ASM International, 13 (1987) 583
3. J. Hatch, editor, *Aluminum Properties and Physical Metallurgy*, Metals Park (OH): ASM, (1984) 58
4. B. Shaw, G. Davis, W. Moshier, G. Long and R. Black, *J. Electrochem. Soc*., 138 (1991) 3288
5. G. Davis, B. Shaw, B. Rees and M. Ferry, *J. Electrochem. Soc.*, 138 (1993) 3194
6. Z. Szklarska-Smialowska, *Corrosion Sci*., 41 (1999) 1743
7. Y. M. Wang, H. H. Kuo and S. Kia, *Plat. Surf. Fin.*, 91 (2004) 34
8. L.H. Chiu, H.A. Lin and C.C. Chen, *Materials Science Forum*, 419 (2003) 909
9. L.H. Chiu, C. C. Chen and C. F. Yang, *Surf. Coat. Tech.*, 191 (2005) 181
10. X.F. Meng, G. Wei, H.L. Ge, Y.D. Yu, Y. Cao and D. Horst, *Int. J. Electrochem. Sci*., 8 (2013) 10660
11. Y.Z. Shen, H.G. Li, H.J. Tao, J. Ling, T. Wang and J. Tao, *Int. J. Electrochem. Sci*., 10 (2015) 938
12. M. Ovundur, F. Muhaffel and H. Cimenoglu, *Tribology in Industry*, 37 (2015) 55
13. R. Ayer , J.Y. Koo, J.W. Steeds and B.K. Park, *Metall. Mater. Trans. A-Phys. Metall. Mater. Sci.*, 16A (1985) 1925
14. H. Ezuber, A. El-Houd and F. El-Shawesh, *Materials and Design*, 29 (2008) 801
15. L. Lacroix, C. Blanc, N. Pebere, G.E. Thompson, B. Tribollet and V. Vivier, *Corrosion Sci.*, 64 (2012) 213
16. J. Idrac, G. Mankowski, G. Thompson, P. Skeldon, Y. Kihn and C. Blanc, *Electrochim. Acta*, 52 (2007) 7626
17. A.Y. Musa, A. B. Mohamad, A. A. H. Kadhum and E. P. Chee, *Int. J. Electrochem. Sci.*, 6 (2011) 5052
18. C. Blanc, N. Pebere, B. Tribollet and V. Vivier, *Corrosion Sci.*, 52 (2010) 991
19. J.-B. Jorcin, C. Blanc, N. Pébère, B. Tribollet and V. Vivier, *J. Electrochem. Soc.*, 155 (2013) C46
20. L.H. Chiu, K. H. Chen, C. Y. Tsai and S. R. Lee, *Advanced Materials Research*, 849 (2014) 14
21. ASTM G71-81, *Standard Guide for Conducting and Evaluating Galvanic Corrosion Tests in Electrolytes*, (2009) 259
22. H. Zhu, X. Zhang, M. J. Couper and A. K. Dahle, *Metall. Mater. Trans. A-Phys. Metall. Mater. Sci.*, 40A (2009) 3264
23. R. Akeret, H. Bichsel, E. Schwall, E. Simon and M. Textor, *Trans. Inst. Metal Finish.*, 67 (1989) 20
24. M.A. Pech-Canul, R. Giridharagopal, M.I. Pech-Canul, and E.E. Coral-Escobar, *J. Mater. Eng. Perform.*, 22 (2013) 3922
25. R.O. Hussein, X. Nie, D.O. Northwood, *Electrochim. Acta*, 112 (2013) 111
26. V. Raj and M. M. Ali, *J. Mater. Process. Technol.*, 209 (2009) 5341
27. M. Garcia-Rubio, P. Ocon, A. Climent-Font, R.W. Smith, M. Curioni, G.E. Thompson, P. Skeldon, A. Lavia and I. Garcia, *Corrosion Sci.*, 51 (2009) 2034
28. F. Brown and W. D. Mackintosh, *J. Electrochem. Soc.*, 120 (8) (1973) 1096
29. G. Patermarakis, *J. Electroanal. Chem.*, 730 (2014) 69
30. B. Zaid, D. Saidi, A. Benzaid and S. Hadji, *Corrosion Sci*., 50 (2008) 1841

31. O.R. Brown and J.S. Whitley, *Electrochim. Acta*, 32 (1987) 545
32. S.I. Pyun, S.M. Moon, S.H. Ahn and S.S. Kim, *Corrosion Sci.*, 41 (1999) 653
33. N. Chaubey, V. K. Singh, Savita and M. A. Quraishi, *Int. J. Electrochem. Sci.*, 10 (2015) 504
34. J. Zhang, M. Klasky and B. C. Letellier, *J. Nucl. Mater.*, 384 (2009) 175
35. F. Balbaud-Celerier and F. Barbier, *J. Nucl. Mater.*, 289 (2002) 227